Computational analysis of thresholds for magnetophosphenes

Ilkka Laakso and Akimasa Hirata

Department of Computer Science and Engineering, Nagoya Institute of Technology, Japan

E-mail: laakso.ilkka@nitech.ac.jp

Abstract. In international guidelines, basic restriction limits on the exposure of humans to low-frequency magnetic and electric fields are set with the objective of preventing the generation of phosphenes, visual sensations of flashing light not caused by light. Measured data on magnetophosphenes, i.e., phosphenes caused by a magnetically induced electric field on the retina, are available from volunteer studies. However, there is no simple way for determining the retinal threshold electric field or current density from the measured threshold magnetic flux density. In this study, the experimental field configuration of a previous study, in which phosphenes were generated in volunteers by exposing their heads to a magnetic field between the poles of an electromagnet, is computationally reproduced. The finite element method is used for determining the induced electric field and current in five different MRI-based anatomical models of the head. The direction of the induced current density on the retina is dominantly radial to the eyeball, and the maximum induced current density is observed at the superior and inferior sides of the retina, which agrees with literature data on the location of magnetophosphenes at the periphery of the visual field. On the basis of computed data, the macroscopic retinal threshold current density for phosphenes at 20 Hz can be estimated as 10 mA m^{-2} ($-20\% \ldots + 30\%$, depending on the anatomical model); this current density corresponds to an induced eddy current of 14 μA ($-20\% \ldots + 10\%$), and about 20% of this eddy current flows through each eye. The ICNIRP basic restriction limit for the induced electric field in the case of occupational exposure is not exceeded until the magnetic flux density is about two to three times the measured threshold for magnetophosphenes, so the basic restriction limit does not seem to be conservative. However, the reasons for the non-conservativeness are purely technical: removal of the highest 1% of electric field values by taking the 99th percentile as recommended by the ICNIRP leads to the underestimation of the induced electric field, and there are difficulties in applying the basic restriction limit for the retinal electric field.

Submitted to: *Phys. Med. Biol.*

1. Introduction

In electromagnetic dosimetry at extremely low frequencies, the induced electric field in the human body is used as the metric for determining the basic restriction limits (ICNIRP 2010, IEEE 2002). The induced electric field can be estimated computationally using numerical methods and anatomically realistic voxel models.

At frequencies below 100 Hz, the basic restriction limit on the electric field is set with the objective of preventing retinal phosphenes (ICNIRP 2010, IEEE 2002), i.e., visual sensations of light not caused by visual stimuli. Phosphenes can be produced by various kinds of mechanical and electric stimuli on the retina (Oster 1970). Magnetophosphenes (or magnetic phosphenes) are phosphenes caused by a magnetically induced electric field on the retina (Marg 1991, Saunders and Jefferys 2007). In addition to the retina, phosphenes may also be generated in the occipital cortex by localized electrical (Brindley and Lewin 1968) or transcranial magnetic stimulation (Marg 1991, Marg and Rudiak 1994, Merabet *et al* 2003). However, the threshold electric field for phosphene generation in the occipital cortex is considerably higher that that in the retina (Marg 1991), so the generation of phosphenes directly in the brain generally requires specialized magnetic stimulators (Marg and Rudiak 1994). In contrast, an electric field that is sufficient for generating retinal phosphenes can be induced by relatively weak magnetic fields (Lövsund *et al* 1980*b*). Therefore, because the retina has the lowest stimulation threshold and can be viewed as a conservative model of the central nervous system (CNS) (Saunders and Jefferys 2007), the basic restriction limits (ICNIRP 2010, IEEE 2002) everywhere in the CNS are based on the threshold electric field in the retina.

One of the most detailed studies on magnetophosphenes and one that has greatly influenced the ICNIRP (2010) guidelines and the IEEE (2002) standard was performed by Lövsund *et al* (1980*b*), who measured the threshold magnetic flux density for phosphene generation in volunteers in the frequency range 10–50 Hz. Because measurements of the induced electric field in the body are not possible, Lövsund *et al* (1980*b*) could not provide measured data on the threshold value, distribution, or direction of the induced electric field on the retina. Several authors have proposed approximations for the electric field threshold values for the generation of phosphenes (Saunders and Jefferys 2007, Wood 2008, Attwell 2003). The threshold electric field for phosphenes in the IEEE (2002) standard has been approximated as 53 mV m^{-1} on the basis of a homogeneous ellipsoidal model exposed to a uniform magnetic field at a flux density obtained from the data of Lövsund *et al* (1980*b*). However, the magnetic field in the exposure scenario in Lövsund *et al* (1980*b*) is not uniform, nor can a homogeneous model take into account the increase in the density of induced current near high-conductivity tissues such as the eyes (Taki *et al* 2003). In the ICNIRP (2010) guidelines the lower limit of the threshold has been assumed to be 50 mV m^{-1} (Saunders and Jefferys 2007), which appears to be based on calculations involving a homogeneous ellipsoid similar to that considered for the IEEE (2002) standard. Wood (2008) obtained a very similar value, 56 mV m^{-1} (95% confidence interval: 2–1330 mV m^{-1}), from a literature analysis.

The exposure scenario in Lövsund *et al* (1980*b*) has been previously investigated computationally by Taki *et al* (2003) using a low-resolution heterogeneous voxel model of the head exposed to a realistic nonuniform magnetic field. On the basis of the results of Taki *et al* (2003), Saunders and Jefferys (2007) have approximated the retinal threshold electric field as 100 mV m^{-1}. Recently Dimbylow (2011), Hirata *et al* (2011), and Ilvonen and Laakso (2009) have studied the induced electric field on the retina; however, they considered only a uniform magnetic field exposure, for which no measured threshold magnetic flux densities are available.

In this study, by using computational methods, we accurately reproduce the exposure scenario studied by Lövsund *et al* (1980*b*). The computations are performed using five different MRI-based anatomical models of the head. Attention is paid to the

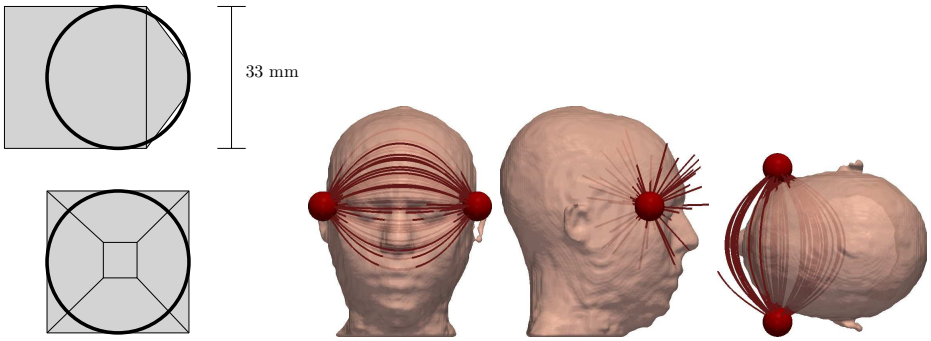

Figure 1. Comparison of the size of the spherical poles with the size of the conical poles used in Lövsund *et al* (1980*b*). The shape of the conical pole has been obtained from Lövsund *et al* (1980*b*, figure 1). The position of the spheres and lines of magnetic flux density for the NORMAN model.

magnitude and direction of the retinal electric field and retinal current density in order to approximate the threshold retinal current/electric field for phosphene generation. The current density on the retina and the current flow induced in the whole head are compared with those determined in previous computational and experimental studies. The induced electric field in the central nervous system is assessed and compared to the ICNIRP (2010) basic restrictions. Finally, we investigate the effects of the voxel size of the computation grid on the numerical accuracy of the computed electric field and current density.

2. Methods and models

2.1. Modelling the exposure setup

In the study of Lövsund *et al* (1980*b*), volunteers were exposed to extremely low frequency magnetic fields by positioning the poles of an electromagnet on the temples. Because Lövsund *et al* (1980*b*) did not provide all dimensions of the conical poles, in this study, the poles of the electromagnet are replaced with two magnetically charged spheres located laterally on each side of the head. The diameter of each sphere is 33 mm, and the spheres have opposite charges. As shown in figure 1, the diameters of the spheres match those of the conical poles. The advantage of spherical approximation is that the magnetic flux density can be calculated analytically.

In Lövsund *et al* (1980*b*), the poles of the electromagnet were located on the temples in the vicinity of the retina. In this work, the spheres were located on a straight lateral line that passes through the median z-coordinate (height) of the eyes and the largest x-coordinate (posterior) of the eyes. The y-coordinate (lateral) of each sphere was as close to the body as possible such that the spheres and the body did not intersect; thus, the spheres and the body were galvanically isolated. The exact distance between the spheres depended on the dimensions of the body model.

The magnetic vector potential between the spheres was calculated analytically by replacing each of the spheres with a (truncated) series of magnetic point charges with the aid of the Kelvin inversion (Jackson 1998). The magnetic vector potential from a

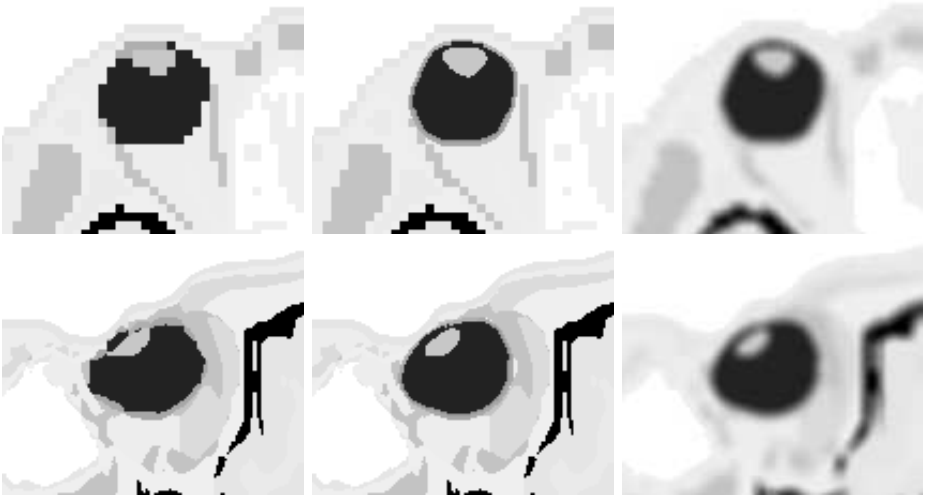

Figure 2. Example of the eyes in the original model (left), the new eye model inserted (middle), and the eyes after smoothing the conductivity (right) for the TARO (top row, horizontal cross section) and ELLA (bottom row, sagittal cross section) models.

point charge was chosen as

$$\mathbf{A} = \frac{Q}{4\pi}\left(\mathbf{u}_\theta \frac{\varphi \sin\theta}{r} + \mathbf{u}_\varphi \frac{1}{r\sin\theta}\right),$$

where the spherical coordinate angles φ and θ were chosen such that the discontinuity in the potential was outside the body.

The magnetic flux density is scaled such that the flux density 2 cm from the surface of each sphere is 10 mT; this value is close to the lowest threshold magnetic flux density for magnetophosphenes, measured by Lövsund *et al* (1980*b*). The frequency is chosen as 20 Hz. Note that the magnitudes of the induced electric field and current depend linearly on the magnetic flux density and frequency (assuming that the conductivity of tissues is independent of the frequency).

In addition to the exposure of the head models to the localized magnetic field between the spheres, their exposure to a uniform lateral magnetic field with a flux density of 10 mT is also considered for comparison.

2.2. Models of the head and eye

A total of five anatomical voxel models of the head were used. The models were the Japanese adult male (TARO) and female (HANAKO) models (Nagaoka *et al* 2004), the Virtual Family adult male (DUKE) and female (ELLA) models (Christ *et al* 2010), and the HPA adult male model NORMAN (Dimbylow 1998). For the TARO, HANAKO, and NORMAN models that consist of 2 mm×2 mm×2 mm voxels, each of the original voxels was divided evenly into 64 new voxels with a 0.5 mm side length. A uniform 0.5 mm×0.5 mm×0.5 mm voxel grid was used for the DUKE and ELLA models. Each of the voxels was assigned a conductivity value, and the assignment of values is discussed in section 2.3.

Before computation, the conductivity is smoothed by averaging it over a sphere with a radius of four voxels (2 mm) (Laakso and Hirata 2012). As shown in section 3.3, the resolution of the computational voxel grid should be finer than the size of the smallest distinguishable geometrical features in order to obtain sound numerical results. After smoothing, the size of the smallest distinguishable geometrical details is approximately 2 mm, which is four times the voxel size (0.5 mm). Smoothing also rounds unrealistic sharp corners in the 2-mm models (TARO, HANAKO, and NORMAN) and removes tiny numerical artefacts such as singular voxels from the DUKE and ELLA models.

None of the models included a model for the retina, and the 2-mm resolution models obviously had very coarse staircase models of the eye. Further, the sclera was discontinuous in the ELLA model. Therefore, an automatic algorithm was used for replacing the original eyes with new ones consisting of sclera, humour, retina, lens, and cornea. Figure 2 shows a comparison of an example of the new eyes with the old eyes of the ELLA and TARO models. For each model, the old eyes were first extracted from the voxel data, after which a surface smoothing algorithm was applied to the outer surface of the eyes. It was ensured that after surface smoothing the volume of the new eyes was equal to that of the original ones. The lenses were treated similarly (the surface was smoothed while keeping the volume intact), after which the new lenses were embedded into the new eyes. Except for the the lens, the conductivity inside the eyeball was assigned to be that of the vitreous humour. The outer voxel layers of the eyeball were divided into sclera, cornea, and retina. Their dimensions were based on literature data (Ogle 1961, Gray 1918). However, because the voxel size was 0.5 mm, and the conductivity was smoothed after the eyes were replaced, it was neither possible nor necessary to reproduce the dimensions precisely. The posterior 5/6 of the eyeball was covered by the sclera with a thickness varying from 0.5 mm (equator) to 1 mm (posterior pole). The anterior 1/6 of the eye was covered by the cornea with a thickness ranging from 0.5 mm (anterior) to 1 mm (periphery). The retina was modelled as a layer with a thickness of one voxel (0.5 mm) located between the sclera and vitreous humour in the posterior 70% of the eye. The choroid tissue, which would be located between the retina and sclera, was not modelled. The same was true for the ciliary body and iris. Finally, the new eyes were embedded back into the voxel models. The voxels that were outside the new eyes but inside the old eyes were treated as fat. With the exception of the eyes, all other tissues were left unchanged.

2.3. Conductivity of tissues

The tissue conductivity values are listed in table 1. The conductivities of ocular tissues and vitreous humour have been taken from the paper of Lindenblatt and Silny (2001). These agree well with the data of Gabriel *et al* (1996). Lindenblatt and Silny (2001) did not perform measurements of the conductivity of the retina, but they deduced by extrapolation from high frequencies (Gabriel *et al* 1983) that the retina should be treated as a high-conductivity tissue. Wood (2008) has commented that the retinal conductivity is actually highly inhomogeneous radially (Brindley 1956) and has argued that using the conductivity of the sclera (0.5 S m^{-1} in that work) would be a practical option for numerical simulations because of the thinness of retinal layers. In this work, the retina has been assigned the conductivity of blood, which falls between the conductivities of the sclera and vitreous humour.

Table 1. Conductivities of tissues. Not all models include all tissues.

Tissue	σ [S m^{-1}]	Tissue	σ [S m^{-1}]
Blood	0.7	Mucous membrane	0.1
Bone (cancellous)	0.07	Muscle	0.35
Bone (cortical) and tooth	0.02	Nerve and spinal chord	0.03
Bone marrow	0.05	Oesophagus	0.5
Brain (grey matter)	0.1	Retina	0.7
Brain (white matter)	0.06	Sclera	0.56
Cartilage	0.18	Skin	0.1
Cerebellum	0.1	Tendon	0.3
Cerebrospinal fluid	1.8	Thyroid and other glands	0.5
Cornea	0.5	Tongue	0.3
Fat	0.04	Trachea	0.3
Lens	0.32	Vitreous humour	1.55

The conductivity of the cerebrospinal fluid has been chosen as 1.8 S m^{-1} (Duck 1990, Baumann *et al* 1997). This value falls between 2.0 S m^{-1} (Gabriel *et al* 1996, Gabriel and Gabriel 1997) and 1.6 S m^{-1} (Grimnes and Martinsen 2008, Gabriel *et al* 2009). The conductivities of other tissues have been obtained from the report of Gabriel and Gabriel (1997) for frequencies lower than 100 Hz. The conductivities of tissues that were not listed in the table of Gabriel and Gabriel (1997) have been derived from other tissue conductivities or from the four Cole-Cole model (Gabriel *et al* 1996). The effects of variations in tissue conductivities on computed results are investigated in section 3.3.

2.4. Determining the induced electric field

As both the frequency and conductivity of the human body are low, the induced electric field in the body depends only on the conductivity of the body and the incident magnetic vector potential. The field can be determined by solving a partial-difference equation for the electric scalar potential (Wang and Eisenberg 1994),

$$\nabla \cdot \sigma \nabla \phi = -\nabla \cdot \sigma \frac{d}{dt} \mathbf{A}_0, \tag{1}$$

where ϕ is the scalar potential, $\mathbf{A}_0$ is the vector potential of the incident magnetic flux density, and σ is the conductivity. The electric field $\mathbf{E}$ can be calculated from ϕ by using the relation $\mathbf{E} = -\nabla\phi - \frac{d}{dt}\mathbf{A}_0$.

In this work, an in-house Matlab code is used for solving the above scalar potential equation numerically. The equation is first discretized using the Galerkin finite element method (FEM) with trilinear node-based basis functions in a uniform grid that coincides with the 0.5 mm cubical voxels of the anatomical models. The elements of the system matrix are calculated analytically, and the terms of the right-hand-side load vector are integrated numerically by applying the first-order Gaussian quadrature (mid-ordinate rule) to each voxel. The resulting linear equation system with about 40 million unknowns is then solved numerically until the relative residual is less than 10^{-10}.

2.5. Analysis of the induced electric field and current

2.5.1. Retinal current density and electric field The geometry around the eyeball consists of a high-conductivity material (vitreous humour) embedded in lower-conductivity tissue (orbital fat, muscle, and skull). The relatively thin layers of sclera, retina, and choroid that separate the eyeball from the surroundings are likely to have a conductivity that is at least as high as the conductivity of the surroundings. Consequently, their conductivities—which may be radially inhomogeneous (Brindley 1956), uncertain, or inaccurate (Attwell 2003)—should have only a small effect on the *tangential* component of the induced electric field and the *radial* component of the induced current density. Therefore, we have reported the results on the retina in terms of the radial current density and the tangential electric field, and the radial electric field and the tangential current density can be calculated from the results by using the conductivity, whatever the value is. The radial (normal) and tangential components on the retina have been approximated by transforming the field from Cartesian coordinates to spherical coordinates with the origin at the centre of each eye.

2.5.2. Total induced current In addition to the localized values of the current and electric field on the retina, the total induced eddy current is investigated globally over the whole head. The induced eddy current is divergence-free, and hence, the current flow can be thought to consist of an infinite number of closed imaginary current loops. The total induced current is the sum of the currents flowing in the loops. In this work, the total induced current has been approximated by calculating the total current flowing upwards (or downwards) for each axial cross section and taking the maximum. The percentage of total current that flows through the eyes has been calculated from the radial component of the current density on the eye surface. If the current were to be divided into imaginary current loops, this would be the percentage of loops that intersect the eyes.

2.5.3. Comparison with basic restriction limits The induced electric field is compared to the basic restriction limits specified by the ICNIRP (2010). The ICNIRP (2010) guidelines first require the vector average of the electric field to be taken over 8 mm^3 cubes, and then taking the 99th percentile of the averaged field in each specific tissue. In this study, the vector average has been calculated by taking the numerical convolution between each component of the induced electric field and a 8 mm^3 cubical volume consisting of 64 voxels. For the brain, the electric field values outside the brain were set to zero for the purpose of averaging. The 99th percentile has been taken over the whole brain because the segmentation of brain tissues is different in each model. In addition to the 99th percentile value, the maximum 8 mm^3-averaged electric field is also reported. For the retina, because of the uncertain retinal conductivity and the approximative nature of the model for the eye, it was not possible to calculate the 8 mm^3-averaged electric field reliably, which is discussed in section 4.4.

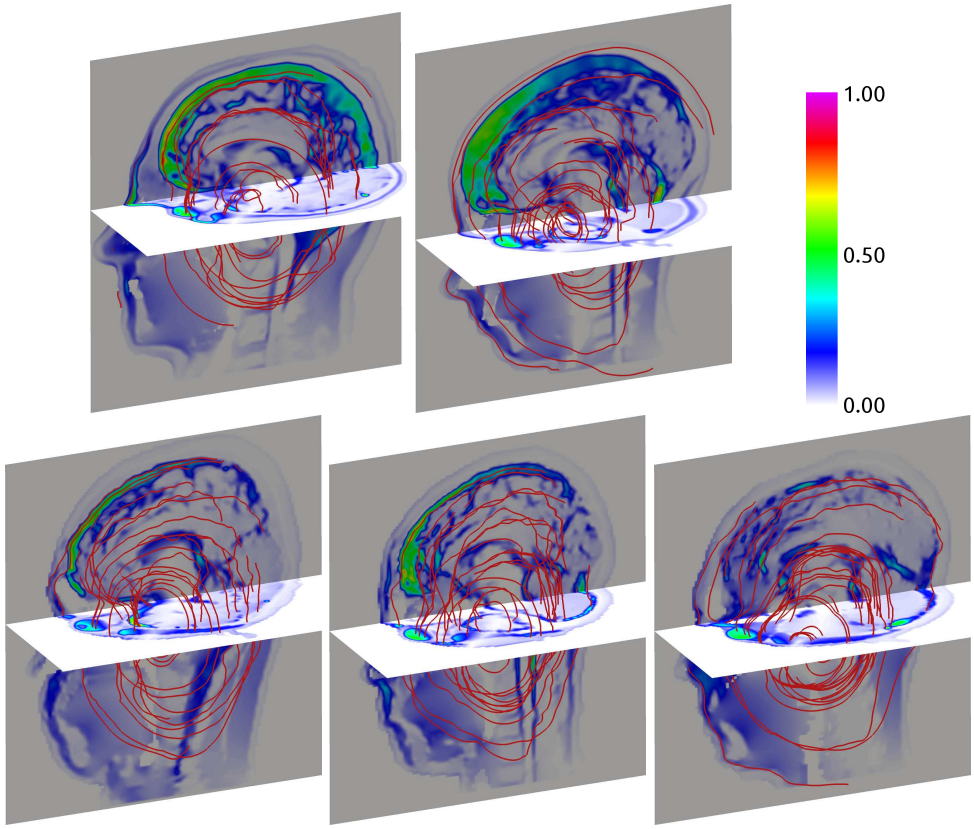

Figure 3. Magnitude and direction (streamlines) of the induced current density on the mid-sagittal cross section and an axial cross section that crosses the eye. For each model, he linear rainbow scale is normalized by the maximum current density. Left to right: DUKE and ELLA (top row), TARO, HANAKO, and NORMAN (bottom row).

3. Results

3.1. Distribution of the induced current

Figure 3 shows the induced current density in the whole head. In the figure, the areas with the highest current density correspond to the location of high-conductivity material such as the cerebrospinal fluid (CSF) and vitreous humour. Although the source of the magnetic field is relatively localized (figure 1), a significant current flow is induced everywhere in the head, for example, in the CSF around the cerebellum that is located far away from the source of the magnetic field.

The current density distribution around the eyes is notably similar in all the models: the current is significantly larger inside the eyeball than in the surrounding tissues because of the high conductivity of the vitreous humour; the current enters (or exits, depending on the phase) the eye on the inferior side, and exits the eye on the superior side. The detailed distribution of the induced current density on the retina is shown in figure 4. In each of the models, the maximum current density—and the maximum electric field—is observed at the superior and inferior peripheries and the

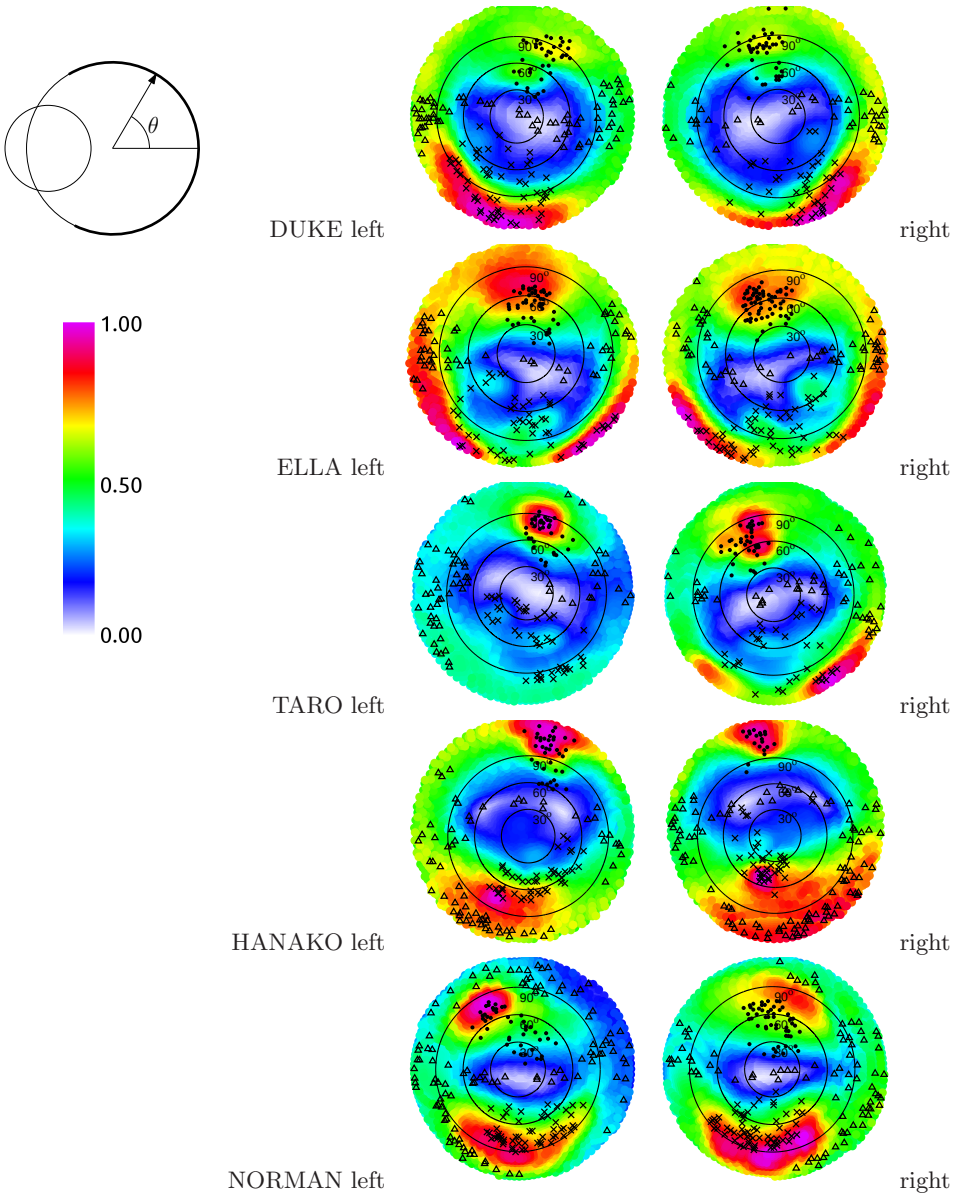

Figure 4. Magnitude of the retinal current density on a linear rainbow scale normalized by the maximum current density on each retina. The angle of $\theta = 0°$ is the posterior pole. The markers show which component of the current is dominant (at least two times greater than the other). The placement of the markers has been chosen randomly such that the markers are distributed more densely in regions with a higher magnitude of current density. Crosses and dots = in and out directions of the radial component, triangles = tangential component. The models are looking in the same direction as the reader.

minimum current density (and the minimum electric field) is seen at the posterior pole, i.e., at the centre of the visual field.

3.2. Induced current in retina and brain

Table 2 shows results for 20 Hz when the magnetic flux density measured 2 cm from the spherical poles is 10 mT. The reported values for the retina are the maximum radial component of the current density and the maximum tangential component of the electric field. Note that the maximum radial current density is almost identical to the maximum absolute value of the retinal current density since the radial component is dominant at the points with the greatest current density (figure 4). Table 2 also shows the total induced eddy current and the percentage of this current that flows through the eyeballs. Differences in the maximum retinal current density between models are mainly because of differences in the total induced eddy current circulating in the head. Indeed, the maximum retinal current density is fairly constant at 0.68–0.84 mA m^{-2} per 1 μA total current, except for the right eye of the TARO model. In the TARO model, the distribution of the retinal current is more localized in the left eye than in the right eye resulting in a higher peak value (figure 4). The same tendency can also be observed for a uniform magnetic flux density (table 3). The reason for this difference is that the distribution of the CSF above the eyes is not symmetric.

Depending on the model, the percentage of total induced eddy current flowing through the eyes can be as high as 30–50%. The variation between the models can be explained by the distribution of other tissues and body fluids in the anterior part of the head. For example, in the axial cross section plane in figure 3, there is a conducting path formed by the CSF posterior to the eyes in the TARO and DUKE models. The ELLA and NORMAN models have no such current path, so a larger portion of the current is channelled through the eyes.

The 99th percentile electric field values in the brain are 15–18 mV m^{-1} in all models other than the NORMAN model, in which it is 28 mV m^{-1}. These values do not exceed the ICNIRP (2010) basic restriction limit for occupational exposure (50 mV m^{-1}). The maximum 8 mm^3-averaged values are close to or exceed 50 mV m^{-1} in all but one model (TARO). The highest electric field values are located in the anterior frontal lobe, immediately above the orbits. The significantly different 99th percentile and maximum electric field values in the NORMAN model compared to other models are caused mainly by modelling artefacts, not by real anatomical differences. Namely, there is almost no CSF in the anterior frontal lobe, where the highest electric field is observed, so the brain is in direct contact with the skull. Also, unlike in other models, the brain is not segmented into grey and white matters. This results in a different current distribution in the brain, which can also be seen in figure 3.

Table 3 shows results for a uniform lateral magnetic flux density of 1.25 mT, which is the reference level specified by the ICNIRP (2010) for occupational exposure. Analysis of the induced fields has been carried out only for the head, but the computation was performed for a 0.5-mm-resolution whole-body model that was truncated at the knee level. The current density and electric field on the retina are generally 60% less than those for the non-uniform exposure (table 2). The 99th percentile and maximum 8 mm^3-averaged electric field values in the brain are in agreement with the ICNIRP (2010) basic restriction limit of 50 mV m^{-1}. Even though the magnetic flux density is uniform, a high percentage of total induced eddy current, as high as 22% to 35%, flows through the eyes.

Table 2. Values of the 99th percentile and maximum 8 mm^3 averaged electric fields in the brain, the maximum radial current density and the maximum tangential electric field on the retinas, and the total induced eddy current in the head along with the percentage of this current flowing through the eyes. The magnetic flux density measured 2 cm from the spherical poles is 10 mT.

	Brain E-field (mV m^{-1})		Radial J (mA m^{-2})		Tangential E (mV m^{-1})		Total current	Eye current
Model	99th perc.	max.	left	right	left	right	(μA)	(% of total)
DUKE	18	53	11	12	9.2	10	16	34
ELLA	15	46	12	11	11	11	16	49
TARO	16	34	14	10	8.0	8.5	17	30
HANAKO	17	54	8.8	8.1	7.8	8.1	11	40
NORMAN	27	82	12	10	10	9.5	14	45

Table 3. The same results as in table 2 but for exposure to a uniform lateral magnetic flux density of 1.25 mT.

	Brain E-field (mV m^{-1})		Radial J (mA m^{-2})		Tangential E (mV m^{-1})		Total current	Eye current
Model	99th perc.	max.	left	right	left	right	(μA)	(% of total)
DUKE	13	27	4.9	5.1	3.2	3.3	9.8	23
ELLA	12	24	5.1	4.6	3.4	3.5	8.3	35
TARO	14	26	6.2	4.4	3.2	2.8	9.7	22
HANAKO	12	25	3.8	3.8	2.6	2.9	6.7	28
NORMAN	15	44	4.2	4.1	3.1	3.0	8.4	28

3.3. Effects of voxel size and variations in tissue conductivity

In order to assess the uncertainty due to the voxel size on the induced electric field and current, simulations were repeated for four voxel sizes (2 mm, 1 mm, 0.5 mm, and 0.25 mm). For voxel sizes of 2 mm and 1 mm, the conductivity of the voxels was determined by taking the arithmetic average of the conductivity over 64 or eight 0.5 mm voxels, respectively. Tissues were classified as brain/retina if more than 1/8 of the voxels belonged to the brain/retina. The higher-resolution (0.25 mm) model was constructed by dividing the 0.5 mm voxels evenly into eight smaller voxels. After the voxel size was changed, the conductivity was smoothed by averaging it over a small sphere, as described in Laakso and Hirata (2012). Smoothing spheres with various radii were used. The size of the smallest distinguishable details in the models after the conductivity was smoothed was approximated by multiplying the voxel size with the smoothing radius.

Tables 4 and 5 show the variation of some computed quantities relative to the reference (0.5 mm resolution, with the conductivity smoothed over a sphere with a radius of four voxels) for the DUKE and ELLA models, respectively. Note that the smallest detail size of 0.5 mm in the first two rows is finer than the resolution of the anatomical images from which the models have been constructed (Christ *et al* 2010). The 99th percentile electric field, the maximum 8 mm^3 cube-averaged electric field, and the retinal current and retinal electric field were stable for different combinations of the voxel size and smoothing, provided that the smallest details (after smoothing) were no larger 2 mm and the voxel size was finer than the smallest details.

Table 4. Effects of voxel size and smoothing on the calculated results for the DUKE model. The values have been scaled to the reference (seventh row). The first column is the approximate size of the smallest distinguishable details after the conductivity has been averaged over a sphere with the radius listed in the third column.

Smallest details (mm)	Voxel size (mm)	Smoothing (voxels)	Brain E-field			Left retina		Total current
			99th perc.	max. (8 mm^3)	max. (voxel)	radial J (max.)	tangential E (max.)	
0.5	0.25	2	0.93	0.89	1.65	1.12	0.99	0.92
0.5	0.5	0	0.92	0.93	1.99	1.18	1.14	0.90
1	0.25	4	0.96	0.87	1.25	1.03	0.96	0.95
1	0.5	2	0.95	0.88	1.20	1.05	0.96	0.94
1	1	0	0.96	0.93	1.22	1.24	0.96	0.93
2	0.25	8	1.00	1.00	1.06	0.99	1.01	1.00
2	0.5	4	1.00	1.00	1.00	1.00	1.00	1.00
2	1	2	1.01	1.00	0.98	1.02	1.02	1.00
2	2	0	1.06	1.54	1.29	1.10	1.03	0.98
4	0.5	8	0.98	0.92	0.98	0.91	1.19	1.09
4	1	4	0.99	0.98	0.99	0.92	1.20	1.09
4	2	2	1.01	1.21	1.01	0.96	1.24	1.09

Table 5. Effects of voxel size and smoothing on the calculated results for the ELLA model. The values have been scaled to the reference (seventh row).

Smallest details (mm)	Voxel size (mm)	Smoothing (voxels)	Brain E-field			Left retina		Total current
			99th perc.	max. (8 mm^3)	max. (voxel)	radial J (max.)	tangential E (max.)	
0.5	0.25	2	0.97	1.00	2.35	1.03	0.91	0.90
0.5	0.5	0	0.96	1.03	2.09	1.12	0.92	0.87
1	0.25	4	0.98	0.96	1.39	1.01	0.96	0.94
1	0.5	2	0.98	0.96	1.21	1.02	0.95	0.93
1	1	0	1.00	1.04	1.22	1.09	0.94	0.91
2	0.25	8	1.00	0.99	1.02	1.00	1.00	1.00
2	0.5	4	1.00	1.00	1.00	1.00	1.00	1.00
2	1	2	1.01	1.04	0.95	0.98	1.00	1.00
2	2	0	1.08	1.05	0.88	1.09	0.98	0.97
4	0.5	8	0.97	0.74	0.70	0.93	1.07	1.10
4	1	4	0.97	0.75	0.68	0.91	1.07	1.10
4	2	2	1.00	0.74	0.63	0.92	1.06	1.10

Since many of the tissue conductivities are uncertain (Gabriel *et al* 2009), the sensitivity of computed results to variations in conductivity was investigated. The conductivities of brain, CSF, or eyes (humour, retina, sclera, cornea, lens) were decreased or increased from the values presented in table 1. For brain tissues, the conductivity was varied in the range from −50% to +100%. For the lower end of the range, −50%, the conductivities of white and grey matter were close to those predicted by Gabriel's four Cole Cole model (Gabriel *et al* 1996). The higher end of the range, +100%, was chosen arbitrarily. Some references suggest even higher conductivities for brain tissues (Grimnes and Martinsen 2008, Gabriel *et al* 2009, Wagner *et al* 2004). For

Table 6. Effects of altered conductivity on the 99th percentile and maximum 8 mm^3 averaged electric fields in the brain, the maximum radial current density and the maximum tangential electric field on the left retina, the total induced eddy current in the head, and the total induced eddy current that flows through the eyes for the DUKE model. The values have been scaled to the reference (table 2).

	Brain E-field		Left retina			
Altered conductivity	99th perc.	max. (8 mm^3)	radial J (max.)	tangential E (max.)	Total current	Eye current
Brain tissues −50%	1.25	1.53	0.96	0.98	0.90	0.93
Brain tissues +100%	0.81	0.64	1.05	1.03	1.16	1.08
CSF −20%	0.98	0.90	0.98	0.99	0.95	0.97
CSF +20%	1.02	1.10	1.02	1.01	1.05	1.02
Eyes −20%	1.00	0.99	0.95	1.11	1.00	0.96
Eyes +20%	1.00	1.01	1.04	0.92	1.00	1.03
Retina = 0.01 S/m	1.00	1.00	0.97	1.01	1.00	0.99

the CSF, the variation range was ±20%, which covered values reported in a wide range of studies (Baumann *et al* 1997, Gabriel *et al* 1996, Gabriel and Gabriel 1997, Wagner *et al* 2004, Grimnes and Martinsen 2008, Gabriel *et al* 2009). For eyes, the variation range was arbitrarily chosen as ±20%. In addition, a retinal conductivity of 0.01 S m^{-1} was considered based on the discussion by Attwell (2003) and Wood (2008).

Table 6 shows the variation of some computed quantities for the DUKE model. The variation was qualitatively similar for all five models. Both the 99th percentile and maximum averaged electric field values in the brain were sensitive to variations in brain conductivity. A higher brain conductivity resulted in lower electric field values, and vice versa. The greatest variations from the reference of 1.00 in the 99th percentile and maximum values were 0.75–1.29 (NORMAN) and 0.64–1.53 (DUKE), respectively. The total induced eddy current was affected moderately by changes in the brain conductivity; as expected, a higher (lower) conductivity always resulted in a larger (smaller) total induced eddy current. The retinal current density was proportional to the total amount of current that flowed through the eyes, but other than that, it seemed to be independent of changes in conductivity values.

4. Discussion

4.1. Estimated phosphene thresholds

Evidence from electrical stimulation experiments suggest that phosphenes result from stimulation of the retina by radial current (Brindley 1955). Therefore, in the following, computationally estimated thresholds are discussed mainly in terms of the radial component of the current density on the retina. Figure 5 shows the estimated phosphene thresholds for the maximum radial current density on the retina and the total induced eddy current in the head as a function of the frequency for different background luminance levels. The thresholds shown in the figure have been determined from the measured threshold magnetic flux density (Lövsund *et al* 1980*b*, figure 2) by scaling the results in table 2 appropriately. Average values for all five head models are shown. From the figure, the lowest threshold for the retinal current density is seen to be 10 mA m^{-2} at 20 Hz in a 1.2 cd m^{-2} background luminance. In terms of the total

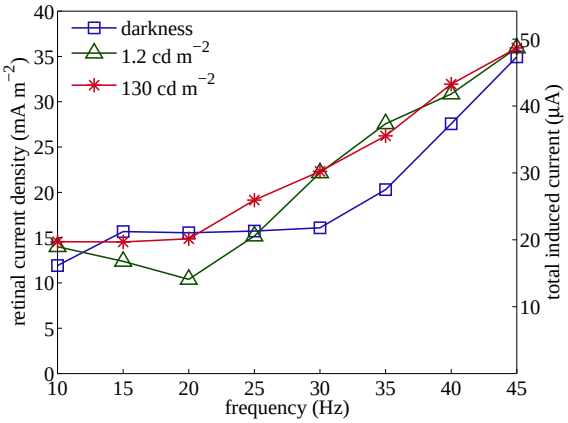

Figure 5. Computed threshold for the maximum retinal current density or total induced current as a function of the frequency and luminosity of the background lighting. Data for the magnetic flux density are taken from the study of Lövsund *et al* (1980*b*).

induced eddy current, the lowest threshold is 14 μA, of which about 20% flows through each eye (40% through both eyes). The range of the variation between the models is $-20\% \ldots +30\%$ for the maximum retinal current density and $-20\% \ldots +10\%$ for the total induced eddy current. These ranges are comparable with the standard deviation of the threshold magnetic flux density between volunteers in the study of Lövsund *et al* (1980*b*).

The estimated threshold current density of 10 mA m^{-2} at 20 Hz is in agreement with the computational estimate of 11 mA m^{-2} obtained by Taki *et al* (2003). The result is also in line with the 10 mA m^{-2} occupational exposure limit in the previous ICNIRP (1998) guidelines. In the new ICNIRP (2010) guidelines, the lowest threshold electric field for phosphenes has been assumed to be 50 mV m^{-1} (Saunders and Jefferys 2007). Considering the retinal conductivity of 0.1 S m^{-1} used by Saunders and Jefferys (2007) would yield a threshold current density of 5 mA m^{-2}, which is conservative compared to the value obtained in this study. The threshold electric field value used by the IEEE (2002) is 53 mV m^{-1}, which is similar to the threshold assumed by ICNIRP (2010). However, it should be noted that the estimated threshold in IEEE (2002) is based on analytic calculations in a homogeneous ellipsoid that can neither take into account the concentration of the induced current in the eyes nor the non-uniformity of the magnetic flux. Wood (2008) and Attwell (2003) have estimated the threshold electric field as 56 mV m^{-1} and 10–60 mV m^{-1}, respectively. However, both authors state that the electric field threshold in the retina has a significant variation range that depends on how the conductivity of the retina is defined (Attwell 2003, Wood 2008).

4.2. Comparison with experimental data

A comparison between different experimental studies is not entirely straightforward as the sensitivity to phosphenes is a complex function of the frequency of stimulation, background lighting, and dark-adaptation state of the eyes (Schwarz 1947, Lövsund

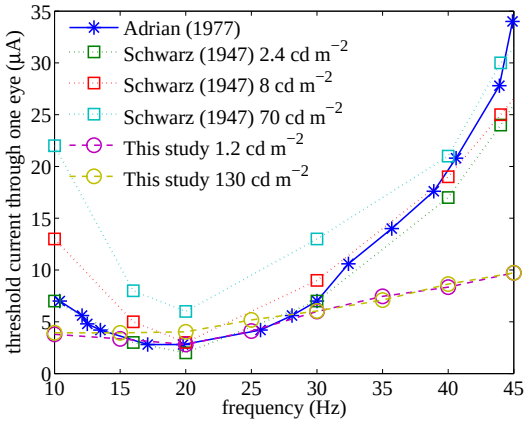

Figure 6. Comparison of experimental threshold currents flowing through one eye for electrophosphenes. Data from the studies of Schwarz (1947, Tabelle 1) and Adrian (1977, Fig. 1) are shown. The portion of current flow through one eye has been approximated as 10% in the study of Schwarz (1947), 20% in the study of Adrian (1977), and 20% in this study.

et al 1980*b*). At the frequency of maximum sensitivity, 20 Hz (Schwarz 1947, Adrian 1977, Lövsund *et al* 1980*a*, Lövsund *et al* 1980*b*), an increase in the luminance of the background light decreases the sensitivity (Schwarz 1947). However, the dependence on the luminance is reversed at frequencies higher than 50 Hz, so an increase in the light level results in an increase in the sensitivity (Schwarz 1947, Carpenter 1972). While dark-adaptation of the eyes shifts the sensitivity maximum to frequencies lower than 20 Hz (also seen in figure 5), the sensitivity to phosphenes also decreases (Schwarz 1947). The sensitivity to phosphenes is also affected by several other factors, such as eye movement, blinking, keeping the eyes open or closed, or repeated application of stimuli (Barlow *et al* 1947, Adrian 1977).

Figure 6 shows a comparison between the computed threshold eddy current for magnetophosphenes and experimental threshold currents for electrophosphenes (Schwarz 1947, Adrian 1977). In the study of Schwarz (1947), the stimulation electrode was positioned between the upper jaw and lip, while the reference electrode was located around the wrist. In the study of Adrian (1977), the stimulation electrode was placed just over the outer edge of the eye and the reference electrode was positioned anterior to the contralateral ear. Schwarz (1947) measured the threshold current for a variety of lighting conditions, while Adrian (1977) carried out measurements in a moderately lit room. We have performed preliminary simulations with simple electrode models, and the results show that the percentage of the stimulation current flowing through one eye is roughly 10% in the study of Schwarz (1947) and 20% in the study of Adrian (1977). These values have been used along with the reported threshold currents to get an approximation for the threshold current flowing through one eye. As figure 6 shows, the measured and computed threshold currents are in a fairly good agreement at and around 20 Hz, but not at higher or lower frequencies. In the studies of both Schwarz (1947) and Adrian (1977), the threshold for electrophosphenes rises sharply at lower and higher frequencies, while the threshold current for magnetophosphenes has a much 'flatter' frequency response. A similar difference in the frequency response between

electro- and magnetophosphenes has been observed by Lövsund *et al* (1980*a*), who reasoned that the difference is because of different current paths or the stimulation of different neural structures in the retina.

Lövsund *et al* (1980*b*) did not provide data about where in the visual field their volunteers observed phosphenes. However, retinal magnetophosphenes are typically the strongest at the periphery and weak or non-existent at the centre of the visual field (Marg 1991, Barlow *et al* 1947, Taki *et al* 2003). Electrical stimulation experiments have shown that the site of stimulation of retinal phosphenes corresponds to the location where the radial component of the current is the strongest (Brindley 1955). In this study, the computed current density was the greatest—and in the radial direction—on the superior and inferior sides of the eyeball, which correspond to the lower and upper peripheries of the visual field, respectively. The minimum occurred at the posterior pole of the eyeball, i.e., at the centre of the visual field. Thus, it appears that the occurrence of magnetophosphenes at the periphery, and not at the centre, of the visual field can be explained only by considering the distribution of the induced current density on the retina.

4.3. Uncertainty due to computational modelling

Contrary to previous reports (Bakker *et al* 2012), we found that both the maximum and 99th percentile electric field averaged over 8 mm^3 cubes were stable for different voxel sizes. However, it was essential for the voxel size to be finer than the smallest distinguishable details. Simply averaging the conductivity over a small sphere with a radius of just two voxels (Laakso and Hirata 2012) was sufficient for removing most variations associated with the voxel size. With the averaged conductivity, the macroscopic retinal radial current density and tangential electric field were very stable for various voxel sizes, unlike the observation in the study of Ilvonen and Laakso (2009), where a significant difference of 50% was observed in electric field values averaged over the whole retina between 1-mm and 2-mm voxel sizes. In this study, while the results were calculated for a 0.5 mm voxel size, it was found that a 1-mm voxel size would have been sufficient for obtaining similar results. It seems clear that the uncertainty associated with the voxel size is considerably less than other uncertainties, for instance, the uncertainties caused by variations between anatomical models or uncertain conductivity values.

The distributions of the induced eddy current in the head and on the retina were qualitatively similar in all five models, but there were significant variations in numerical values between the models. It is difficult to determine whether these variations are caused by real anatomical differences or numerical artefacts introduced in the process of generating the models from magnetic resonance images. It is likely that modelling artefacts are the reason why the maximum and 99th percentile electric fields in the brain of the NORMAN model were much higher than those in other four models. Also, observed differences in the retinal current density between left and right eyes especially in the TARO model could originate from modelling artefacts. On the contrary, it seems that real differences in the size of the head can help to explain the variations in the total induced eddy current. This current was strongly related to the retinal current density and electric field, and it was found to be fairly independent of the voxel size, the amount of distinguishable details, and the conductivity of tissues. For an idealized scenario, such as a sphere exposed to a uniform magnetic field, the total induced eddy current is proportional to the volume of the sphere. The same

Table 7. Comparison with previous computational studies. The present results have been scaled to match the exposure scenario in each of the previous studies. Similarly to previous studies, the 99th percentile values for the retina have been calculated from the non-averaged electric field. LAT = uniform lateral magnetic flux density.

			Electric field (mV m^{-1})	
Model and reference	Exposure setup	Tissue	Reference	This study
TARO	LAT 1 mT/50 Hz	brain, 99th perc.	28.5	28
(Hirata *et al* 2011)	LAT 8.14 mT/20 Hz	retina, 99th perc.	62	59*
NORMAN	LAT 1 mT/50 Hz	brain, 99th perc.	31.6	30
(Dimbylow 2011)	LAT 1 mT/50 Hz	retina, 99th perc.	14	16*
Simple voxel model	Electromagnet/20 Hz	retina, maximum	22*	13–21*
(Taki *et al* 2003)	LAT 5 mT/20 Hz	retina, maximum	34*	30–50*

* Assuming a retinal conductivity of 0.5 S m^{-1}.

tendency seems to apply for the realistic case: if the total current is divided by the volume of the brain (which correlates with the head size), the variation range between models is reduced from 11–17 μA to 11–13 (μA per 1 L brain volume).

The computed 99th percentile and retinal electric fields agree very well with those obtained in previous computational studies (table 7). In each of the previous studies, the size of the head and the conductivity of the eyes were similar to those in this study, and hence, the total eddy current and the portion of this current flowing through the eyes are likely to be relatively similar in all studies; this explains the good agreement between the present study and past studies with regard to the retinal electric field and current.

In table 7, the retinal electric field has been calculated from the current density by considering a conductivity of 0.5 S m^{-1}, which was the conductivity of the sclera used in previous studies. From a macroscopic dosimetric viewpoint, the use of the same conductivity for both sclera and retina is well justified for numerical simulations (Wood 2008). However, it should be noted that the conductivity of the retina is not constant in the radial direction (Brindley 1956), as discussed by Wood (2008), so the radial electric field will vary across the retina. Consequently, the radial electric field obtained from the current density by considering a homogeneous conductivity value—any value between 0.01–1.5 S m^{-1} (Attwell 2003, Wood 2008)—is an effective macroscopic field that should not be used for determining threshold values of the microscopic electric field in the retina. If no information on the microscopic conductivity inside retina is available, it is preferable to report the results in terms of the macroscopic retinal current density, which is dominantly radial to the eyeball. Therefore, the magnitude of the retinal current density is almost independent of the retinal conductivity, which is also seen in table 6.

The present computational model did not include small-scale blood vessels in the sclera, retina, and the surroundings. Previously, on the basis of a computational model, Lindenblatt and Silny (2002) have proposed that the concentration of current at small blood vessels can cause significant 'hotspots' in the retinal electric field. However, the hotspots predicted by the model are not supported by the experimental data of Brindley (1955), who observed the uniform distribution of phosphenes in the visual field (except a slightly brighter patch at the macula and a ring at the optic disc)

upon stimulating the eye with a 50-Hz current from a corneal electrode.

4.4. Comparison with basic restriction limits

In the experiments by Lövsund *et al* (1980*b*), non-uniform magnetic fields at frequencies of 10–50 Hz were used for inducing magnetophosphenes in humans. At a frequency of 20 Hz, the threshold magnetic flux density for eliciting magnetophosphenes was found to be about 10 mT (measured 2 cm from the poles of the electromagnet). Because the basic restriction limit in the ICNIRP (2010) guidelines is set with the objective of preventing the generation of phosphenes, it is clear that in this particular experimental field configuration, the internal electric fields should violate the basic restriction limit. In this study, the dosimetry of the induced electric field was performed using a computational model that closely mimics the experimental setup. It turned out that, for the threshold magnetic flux density, the internal fields in the brain and retina (see below) were *in compliance* with the basic restriction limit. Actually, the basic restriction limit was not exceeded until the magnetic flux density was increased to 20–30 mT, which is two to three times the measured threshold. Therefore, it would appear that the ICNIRP (2010) basic restriction limit is not sufficient for the prevention of magnetophosphenes. The reasons for this non-conservativeness are technical difficulties in applying the basic restriction limit.

The exposure scenario is localized, so the 99th percentile may result in a considerable underestimation of the real exposure (Laakso and Hirata 2012). Indeed, the maximum value of the electric field averaged over 8 mm^3 cubes in the brain was higher than the 99th percentile by a factor of two to three. For the threshold magnetic flux density, the maximum averaged electric fields were close to or exceeded the basic restriction limit of 50 mV m^{-1} in all but one model. This raises the question of whether it would be more appropriate to define the basic restriction limit as the maximum value (within any 8 mm^3 cube) instead of the 99th percentile value. However, it should be noted that both the 99th percentile and maximum electric field values in the brain may be affected significantly by the uncertainty in the conductivity of the brain (table 6).

Another problem is related to the averaging of the electric field on the retina. The ICNIRP (2010) guidelines recommend that the 8 mm^3 averaging cube "may extend to the tissues in front and behind the retina". This is problematic because the electric field is discontinuous near the retinas. For instance, a current density of 10 mA m^{-2} in the radial direction would give an electric field of 18 mV m^{-1} in the sclera and 250 mV m^{-1} in the orbital fat. Consequently, the averaged electric field depends strongly on the thicknesses of retina, choroid, and sclera. Because the resolution of 0.5 mm was insufficient for representing these layers accurately, the reliability of the averaged electric field was poor (and, actually, the 99th percentile and maximum electric field values averaged in this way were generally less than or equal to those in the brain). A more reliable estimate for the retinal electric field could be obtained by first determining the retinal current density and then dividing the current density by an effective conductivity value. For comparison with the basic restriction limit, a suitable effective conductivity for the retina might be 0.2 S m^{-1}, which would result in violation of the basic restriction limit for the 10 mT non-uniform exposure (table 2), but the reference level exposure (table 3) would still be in compliance with the basic restriction limit.

5. Conclusions

The induced electric field and current in five anatomically realistic voxel models of the head were calculated in an exposure scenario similar to that considered in Lövsund *et al* (1980*b*). Exposure to the electromagnet at a magnetic flux density of 10 mT (2 cm from the poles) at 20 Hz induces an eddy current of 11–17 μA, depending on the anatomical model, that circulates in the head. A significant portion, up to 30–50%, of the total current tends to flow through the eyes because of the higher conductivity of the eyes compared to the surrounding tissues. The induced current density on the retina is dominantly radial to the eyeball, and the maximum induced current density is found at the superior and inferior sides of the retina. The maximum macroscopic retinal current density in different anatomical models varies between 9–14 mA m^{-2}, where the variation is mainly caused by differences in the total induced eddy current. From a comparison with the threshold magnetic flux density measured by Lövsund *et al* (1980*b*), the lowest macroscopic retinal threshold current density for phosphenes at 20 Hz can be estimated as 10 mA m^{-2}, radial to the eyeball.

The induced electric field at the measured threshold magnetic flux density for magnetophosphenes did not exceed the ICNIRP (2010) basic restriction limit for occupational exposure in the brain or retina. This suggests that the basic restriction limit is not conservative for preventing phosphenes for localized magnetic field exposure. However, as we have pointed out earlier (Laakso and Hirata 2012), the 99th percentile may greatly underestimate the maximum induced field for localized exposure. Indeed, the basic restriction limit would be conservative if the 99th percentile were to be replaced by the maximum value of the electric field averaged over 8 mm^3 cubes. Additionally, there are difficulties in reliably calculating the 8 mm^3 averaged electric field on the retina. We also found that the computational results did not depend significantly on the voxel size, provided the voxel size was 1 mm or less and the conductivity was 'smoothed' (Laakso and Hirata 2012) such that the computational voxel size was finer than the size of the smallest distinguishable geometrical details.

Acknowledgements

The authors wish to thank the Finnish Cultural Foundation and the Academy of Finland for financial support.

References

Adrian D J 1977 Auditory and visual sensations stimulated by low-frequency electric currents *Radio Sci.* **12**(6S) 243–50

Attwell D 2003 Interaction of low frequency electric fields with the nervous system: The retina as a model system *Radiation Protection Dosimetry* **106**(4) 341–8

Bakker J F, Paulides M M, Neufeld E, Christ A, Chen X L, Kuster N and van Rhoon G C 2012 Children and adults exposed to low-frequency magnetic fields at the ICNIRP reference levels: theoretical assessment of the induced electric fields *Phys. Med. Biol.* **57**(7) 1815–29

Barlow H B, Kohn H I and Walsh G E 1947 Visual sensations aroused by magnetic fields *American Journal of Physiology* **148**(2) 372–5

Baumann S, Wozny D, Kelly S and Meno F 1997 The electrical conductivity of human cerebrospinal fluid at body temperature *IEEE Trans. Biomed. Eng.* **44**(3) 220–3

Brindley G S 1955 The site of electrical excitation ot the human eye *J. Physiol.* **127** 189–200

Brindley G S 1956 The passive electrical properties of the frog's retina, choroid and sclera for radial fields and currents *J. Physiol.* **134**(2) 339–52

Brindley G S and Lewin W S 1968 The sensations produced by electrical stimulation of the visual cortex *J. Physiol.* **196** 479–93

Carpenter R H S 1972 Electrical stimulation of the human eye in different adaptational states *J. Physiol.* **221** 137–48

Christ A, Kainz W, Hahn E G, Honegger K, Zefferer M, Neufeld E, Rascher W, Janka R, Bautz W, Chen J, Kiefer B, Schmitt P, Hollenbach H P, Shen J, Oberle M, Szczerba D, Kam A, Guag J W and Kuster N 2010 The Virtual Family—development of surface-based anatomical models of two adults and two children for dosimetric simulations *Phys. Med. Biol.* **55**(2) N23–38

Dimbylow P 2011 Spherical polar co-ordinate calculations of induced fields in the retina and head for applied magnetic fields at 50 Hz *Phys. Med. Biol.* **56**(14) 4597–611

Dimbylow P J 1998 Induced current densities from low-frequency magnetic fields in a 2 mm resolution, anatomically realistic model of the body *Phys. Med. Biol.* **43**(2) 221–30

Duck F A 1990 Physical properties of tissue: A comprehensive reference book (Edinburgh, UK: Academic)

Gabriel C and Gabriel S 1997 Compilation of the dielectric properties of body tissues at RF and microwave frequencies, Physics Department, King's College, London, UK
URL: *http://niremf.ifac.cnr.it/docs/DIELECTRIC/home.html*

Gabriel C, Peyman A and Grant E H 2009 Electrical conductivity of tissue at frequencies below 1 MHz *Phys. Med. Biol.* **54**(16) 4863–78

Gabriel C, Sheppard R J and Grant E H 1983 Dielectric properties of ocular tissues at 37 degrees C *Phys. Med. Biol.* **28**(1) 43–9

Gabriel S, Lau R W and Gabriel C 1996 The dielectric properties of biological tissues: III. Parametric models for the dielectric spectrum of tissues *Phys. Med. Biol.* **41**(11) 2271–93

Gray H 1918 Anatomy of the human body (Philadelphia, PA: 20th ednLea & Febiger)

Grimnes S and Martinsen Ø G 2008 Bioimpedance and bioelectricity basics (Oxford, UK: 2nd ednElsevier)

Hirata A, Takano Y, Fujiwara O, Dovan T and Kavet R 2011 An electric field induced in the retina and brain at threshold magnetic flux density causing magnetophosphenes *Phys. Med. Biol.* **56**(13) 4091–101

ICNIRP 1998 Guidelines for limiting exposure to time-varying electric, magnetic and electromagnetic fields (up to 300 GHz) *Health Phys.* **74**(4) 492–522

ICNIRP 2010 Guidelines for limiting exposure to time-varying electric and magnetic fields (1 Hz to 100 kHz) *Health Phys.* **99**(6) 818–36

IEEE 2002 IEEE Standard for Safety Levels with Respect to Human Exposure to Electromagnetic Fields, 0-3 kHz, C95.6-2002 (New York: Institute of Electrical and Electronics Engineers)

Ilvonen S and Laakso I 2009 Computational estimation of magnetically induced electric fields in a rotating head *Phys. Med. Biol.* **54**(2) 341–51

Jackson J D 1998 Classical electrodynamics (New York: 3rd ednJohn Wiley & Sons)

Laakso I and Hirata A 2012 Reducing the staircasing error in computational dosimetry of low-frequency electromagnetic fields *Phys. Med. Biol.* **57**(4) N25–N34

Lindenblatt G and Silny J 2001 A model of the electrical volume conductor in the region of the eye in the ELF range *Phys. Med. Biol.* **46**(11) 3051–59

Lindenblatt G and Silny J 2002 Electrical phosphenes: on the influence of conductivity inhomogeneities and small-scale structures of the orbita on the current density threshold of excitation *Med. Biol. Eng. Comput.* **40** 354–9

Lövsund P, Öberg P Å and Nilsson S E G 1980*a* Magneto- and electrophosphenes: a comparative study *Med. Biol. Eng. Comput.* **18**(6) 758–64

Lövsund P, Öberg P Å, Nilsson S E G and Reuter T 1980*b* Magnetophosphenes: a quantitative analysis of thresholds *Med. Biol. Eng. Comput.* **18**(3) 326–34

Marg E 1991 Magnetostimulation of vision: Direct noninvasive stimulation of the retina and the visual brain *Optometry and Vision Science* **68**(6) 427–40

Marg E and Rudiak D 1994 Phosphenes induced by magnetic stimulation over the occipital brain: Description and probable site of stimulation *Optometry and Vision Science* **71**(5) 301–11

Merabet L B, Theoret H and Pascual-Leone A 2003 Transcranial magnetic stimulation as an investigative tool in the study of visual function. *Optometry and Vision Science* **80**(5) 356–68

Nagaoka T, Watanabe S, Sakurai K, Kunieda E, Watanabe S, Taki M and Yamanaka Y 2004 Development of realistic high-resolution whole-body voxel models of Japanese adult males and females of average height and weight, and application of models to radio-frequency electromagnetic-field dosimetry *Phys. Med. Biol.* **49**(1) 1–15

Ogle K 1961 Optics: An introduction for ophthalmologists (Springfield, IL: Charles C. Thomas)

Oster G 1970 Phosphenes *Sci. Am.* **222**(2) 82–7

Saunders R D and Jefferys J G R 2007 A neurobiological basis for ELF guidelines *Health Phys.* **92**(6) 596–603

Schwarz F 1947 Über die elektrische Reizbarkeit des Auges bei Hell- und Dunkeladaptation *Pflügers Archiv European Journal of Physiology* **249** 76–86

Taki M, Suzuki Y and Wake K 2003 Dosimetry considerations in the head and retina for extremely low frequency electric fields *Radiation Protection Dosimetry* **106**(4) 349–56

Wagner T, Zahn M, Grodzinsky A and Pascual-Leone A 2004 Three-dimensional head model simulation of transcranial magnetic stimulation *IEEE Trans. Biomed. Eng.* **51**(9) 1586–98

Wang W and Eisenberg S 1994 A three-dimensional finite element method for computing magnetically induced currents in tissues *IEEE Trans. Magnetics* **30**(6) 5015 –23

Wood A W 2008 Extremely low frequency (ELF) electric and magnetic field exposure limits: Rationale for basic restrictions used in the development of an Australian standard *Bioelectromagnetics* **29**(6) 414–28